Biochem. J. (2012) **448**, 401–407 (Printed in Great Britain) doi:10.1042/BJ20121359

online data

The substrate/product-binding modes of a novel GH120 β-xylosidase (XylC) from *Thermoanaerobacterium saccharolyticum* JW/SL-YS485

Chun-Hsiang HUANG*[1], Yu SUN†[1], Tzu-Ping KO‡, Chun-Chi CHEN§, Yingying ZHENG*, Hsiu-Chien CHAN*, Xuefei PANG*, Juergen WIEGEL‖[2], Weilan SHAO†[2] and Rey-Ting GUO*[2]

*Industrial Enzymes National Engineering Laboratory, Tianjin Institute of Industrial Biotechnology, Chinese Academy of Sciences, Tianjin 300308, China, †Biofuels Institute, School of Environment, Jiangsu University, Zhenjiang 212013, China, ‡Institute of Biological Chemistry, Academia Sinica, Taipei 11529, Taiwan, §CAS Key Laboratory of Pathogenic Microbiology and Immunology, Institute of Microbiology, Chinese Academy of Sciences, Beijing 100101, China, and ‖Department of Microbiology, University of Georgia, Athens, GA 30602-2605, U.S.A.

Xylan-1,4-β-xylosidase (β-xylosidase) hydrolyses xylo-oligomers at their non-reducing ends into individual xylose units. Recently, XylC, a β-xylosidase from *Thermoanaerobacterium saccharolyticum* JW/SL-YS485, was found to be structurally different from corresponding glycosyl hydrolases in the CAZy database (http://www.cazy.org/), and was subsequently classified as the first member of a novel family of glycoside hydrolases (GH120). In the present paper, we report three crystal structures of XylC in complex with Tris, xylobiose and xylose at 1.48–2.05 Å (1 Å = 0.1 nm) resolution. XylC assembles into a tetramer, and each monomer comprises two distinct domains. The core domain is a right-handed parallel β-helix (residues 1–75 and 201–638) and the flanking region (residues 76–200) folds into a β-sandwich domain. The enzyme contains an open carbohydrate-binding cleft, allowing accommodation of longer xylo-oligosaccharides. On the basis of the crystal structures and in agreement with previous kinetic data, we propose that XylC cleaves the glycosidic bond by the retaining mechanism using two acidic residues Asp^{382} (nucleophile) and Glu^{405} (general acid/base). In addition to the active site, nine other xylose-binding sites were consistently observed in each of the four monomers, providing a possible reason for the high tolerance of product inhibition.

Key words: crystal structure, glycoside hydrolase, synchrotron radiation, *Thermoanaerobacterium saccharolyticum*, xylan, β-xylosidase.

INTRODUCTION

Xylans, the most abundant hemicellulosic heteropolysaccharides in plant cell wall, have to be efficiently decomposed into constituent sugars before they can be utilized as a biofuel substrate and other feedstock commodities [1]. The enzymatic strategies for complete destruction of xylan require a number of xylanolytic enzymes with different activities because of the structural complexity of xylan. These xylan-degrading enzymes, including endo-1,4-β-xylanases (EC 3.2.1.8), acetylxylan esterases (EC 3.1.1.72), feruloyl esterases (EC 3.1.1.73), α-L-arabinofuranosidases (EC 3.2.1.55) and α-glucuronidases (EC 3.2.1.139), act synergistically to efficiently release the substituted group, such as ferulic acid, acetic acid, arabinose and glucuronic acid, from a repeating β-1,4-linked xylose backbone to produce short xylo-oligosaccharides. Eventually, the xylo-oligosaccharides are hydrolysed by β-D-xylosidase (EC 3.2.1.37) to yield xylose units [2]. To date, 102 β-xylosidases have been characterized. There are 48, 4, 9, 33, 6, 1 and 1 β-xylosidases belonging to GH (glycoside hydrolase) family 3, 30, 39, 43, 52, 54 and 116 respectively (see CAZy, the carbohydrate-active enzymes database, at http://www.cazy.org/Glycoside-Hydrolases.html, accessed July 2012) [3]. Nowadays, most β-xylosidases suitable for industrial application and processes are thermophilic enzymes because of their unique thermostability features. Nevertheless, only a few β-xylosidases from anaerobic thermophilic bacteria have been reported [4].

Thermoanaerobacterium saccharolyticum JW/SL-YS485 is a highly xylanolytic anaerobic thermophile that grows within a broad pH range (3.85–6.35) and over a broad temperature range (30–66 °C), and can use xylan as the sole carbon and energy source. Several hemicellulolytic enzymes from this bacterial species have been purified and characterized, including one large and cell-associated endoxylanase [5], one glucuronidase [6], two acetylxylan esterases [7] and three xylosidases (XylA, XylB and XylC) [4,8]. However, XylA cannot be classified to any GH family as the gene encoding XylA has yet to be sequenced and cloned [4]. XylB is composed of a 500-residue mature protein and shows 91 % and 35 % protein sequence identity with XynB and XylB from *T. saccharolyticum* and *Caldicellosiruptor saccharolyticus* respectively [8]. XylB was assigned to the GH39 family. XylC has drawn much attention since its discovery because of several aspects. First, no similar xylosidase sequences has been identified, whereas BlastP searches of the XylC protein sequence against the non-redundant protein sequences database have suggested that its novel structural features indicate that it is a new glycosyl hydrolase. Thus XylC has been classified recently as the first member of the new glycohydrolase family GH120 [4]. Secondly, XylC appears to be less sensitive to product inhibition by xylose and may well be functional in

Abbreviations used: AmHyp2, *Acaryochloris marina* hypothetical protein; BaXylB, *Bifidobacterium adolescentis* XylB; BfHyp1, *Butyrivibrio fibrisolvens* hypothetical protein; BlXyl, *Bifidobacterium longum* xylosidase; GH, glycoside hydrolase; MIR, multiple isomorphous replacement; MR, molecular replacement; *p*NP, *p*-nitrophenyl; RiHyp3, *Roseburia intestinalis* hypothetical protein; TsXylC, *Thermoanaerobacterium saccharolyticum* XylC.

[1] These authors contributed equally to this work.

[2] Correspondence may be addressed to any of these authors (email juergenwiegel@gmail.com, weilanshao@gmail.com or guo_rt@tib.cas.cn).

The atomic co-ordinates and structural factors for the wild-type *Thermoanaerobacterium saccharolyticum* JW/SL-YS485 XylC in complex with Tris (code 3VST), xylobiose (code 3VSU) and xylose (code 3VSV) have been deposited in the RCSB PDB.

the presence of high product concentrations that are usually found in industrial applications. To investigate the substrate specificity of XylC, a series of oligosaccharides were tested for the enzyme's activity, including xylobiose, xylotriose, *p*NP-xyloside (*p*NP is *p*-nitrophenyl), *p*NP-α-L-arabinofuranoside, *p*NP-α-D-xylopyranoside, *p*NP-α-D-glucopyranoside, oat spelt xylan, birchwood xylan and carboxymethyl cellulose. The results indicate that only xylobiose, xylotriose and *p*NP-xyloside are preferred substrates [4]. As mentioned above, XylC showed low product inhibition, with approximately 70 % of XylC activity retained at a xylose concentration of 200 mM by using the artificial substrate *p*NP-xyloside [4]. Taken together, these properties render XylC a potent tool for industrial applications. Solving the crystal structure not only will reveal the catalytic mechanism of XylC, but also can provide a basis for the rational engineering of this novel GH120 family enzyme.

MATERIALS AND METHODS

Protein expression, purification, crystallization and data collection

The expression and purification methods employed for the protein have been described previously [4,9]. The wild-type XylC crystals were grown in 0.2 M sodium citrate (pH 5.6) and 15–17 % (w/v) poly(ethylene glycol) 3350 [9]. To prepare heavy-atom derivatized crystals, 15 different mercury compounds of the Heavy Atom Screen Hg kit (Hampton Research) were dissolved (final concentration 2 mM) in the cryoprotectant solution [0.2 M sodium citrate (pH 5.6), 18 % (w/v) poly(ethylene glycol) 3350 and 15 % (w/v) glycerol]. The crystals were soaked in the mercury-containing cryoprotectant for at least 1 h. Seven mercury datasets were collected for solving phase using the MIR (multiple isomorphous replacement) method. The XylC–xylose and XylC–xylobiose crystals were obtained by soaking the wild-type crystals with the cryoprotectant solution which contained 200 mM xylose and 50 mM xylobiose respectively.

The X-ray diffraction datasets from the mercury-derivatized crystals and three complex crystals (with Tris, xylose and xylobiose), were collected to 1.48–2.5 Å (1 Å = 0.1 nm) resolution, at the beamline BL13B1 of the National Synchrotron Radiation Research Center (NSRRC, Taiwan) and at the beamline BL17U of the Shanghai Synchrotron Radiation Facility (SSRF, Shanghai, China). The data were processed using the HKL2000 program [10]. Before structural refinements, 5 % randomly selected reflections were set aside for calculating R_{free} as a monitor [11].

Structural determination and refinement

The XylC crystal structure was solved using a modified MIR method, which we have used in solving other structures [12–15]. Basically, the crystals were soaked with several mercury-containing compounds which can bind to cysteine residues and they turned out to be sufficient in providing good phasing power. The MIR datasets of mercury-containing derivatives were collected at wavelengths of 1.0000 Å (BL13B1) and 0.9793 Å (BL17U). When any four of the seven mercury datasets were combined with the native dataset for phase calculation, up to 2213 amino acids (total 2552 amino acids) were auto-built with the FOM (figure of merit) ranging from 0.19 to 0.41 and the *Z*-scores from 6.32 to 61.53 using SOLVE and RESOLVE [16–19]. The best results were obtained using the datasets of mersalyl acid, mercury acetate, phenylmercury acetate and tetrakis(acetoxymercuri)methane.

The electron density was improved further and the polypeptide tracings became continuous after preliminary refinement using Refmac5 [20], and a complete model with virtually all side chains was built using ARP/wARP [21]. The complex structures (XylC–Tris, XylC–xylobiose and XylC–xylose) were determined by using the MR (molecular replacement) method with PHASER [22]. The $2F_o - F_c$ difference Fourier map showed clear electron densities for most amino acid residues. Subsequent refinements by incorporating ligands and water molecules were according to a 1.0σ map level. The structural refinements were finalized using Coot [23] and CNS [24]. Some data collection and refinement statistics of these crystals are summarized in Table 1 and Supplementary Table S1 http://www.biochemj.org/bj/448/bj4480401add.htm. All Figures were prepared using PyMOL (http://www.pymol.org).

Mutant production and specific activity measurement

Site-directed mutagenesis was performed by inverse PCR and circulation of PCR products using the wild-type xylosidase gene in the expression plasmid pHsh-*xylC* [4]. Xylosidase activity is given in units, the amount of enzyme that releases 1 μmol of product per min, and the specific activity is defined as the number of enzyme units per mg of protein. Protein concentrations were determined by absorbance at 280 nm, and an absorption coefficient of 124025 $M^{-1} \cdot cm^{-1}$ for XylC was obtained by the ProtParam tool from the Expasy server (http://web.expasy.org/protparam/). The β-xylosidase activity was determined by assaying the amount of *p*-nitrophenol released from the artificial substrate *p*NP-xyloside as described previously [4]. The reaction mixture contained 10 μl of properly diluted enzyme (approximately 0.01 unit of XylC and its mutants), 180 μl of 0.1 M potassium phthalate buffer (pH 6.0) and 10 μl of 40 mM *p*NP-β-D-xylopyranoside. After incubation at 65 °C for 5 min, the reaction was stopped by adding 0.6 ml of 1 M Na_2CO_3, and the A_{405} was read. A standard curve was prepared using *p*-nitrophenol.

RESULTS AND DISCUSSION

The overall structure

There are four XylC monomers in an asymmetric unit, forming a tetramer. The contact interface encompasses six protein segments, including residues 53–59, 177–179, 276–305, 449–466, 509–519 and 584–596 (Figures 1A and 1D), that buries a total surface area of 4330 $Å^2$ on each monomer. A PDBePISA analysis shows a CSS (Complex Formation Significance Score) (which ranges from 0 to 1) of 0.978, also indicating that the tetramer formation is not a result of crystal packing [25].

We present three XylC complex structures (XylC–Tris, XylC–xylobiose and XylC–xylose). Initially, a Tris ion was observed in each monomer in the 'native' structure, occupying the active site. It appeared to mimic the substrate/product oligosaccharide as seen in a previous case of β-glucanase [26]. To obtain an apo-form structure, the Tris buffer was changed to either Hepes or citrate buffer. However, a Hepes or citrate ion still bound to the same site as Tris did (results not shown). The protein molecules in XylC–xylobiose and XylC–xylose complexes, solved by MR using XylC–Tris as a search model, also adopt the closed conformation as does XylC–Tris, and all three structures superimpose very well, with RMSDs (root mean square deviations) ranging from 0.108 to 0.145 Å for all Cα atoms.

XylC, like the other β-xylosidases (e.g. in the GH39 and GH43 families), has an open oligosaccharide-binding cleft (Figure 1B). The space of that active site seems to allow only two xylose units to enter and bind (Supplementary Figure S1 at http://www.biochemj.org/bj/448/bj4480401add.htm).

Table 1 Summary of data processing and refinement statistics

Values in parentheses are for the highest resolution shell. $R_{merge} = \Sigma_{hkl}\Sigma_i|I_i(hkl) - <I(hkl)>|\Sigma_{hkl}\Sigma_i I_i(hkl)$.

Parameter	XylC–Tris (PDB code 3VST)	XylC–xylobiose (PDB code 3VSU)	XylC–xylose (PDB code 3VSV)
Data collection			
Wavelength (Å)	1.00	1.00	1.00
Resolution (Å)	25–1.75 (1.81–1.75)	25–2.05 (2.12–2.05)	25–1.48 (1.53–1.48)
Space group		$P2_1$	
Unit cell			
$a/b/c$ (Å)	88.64/202.24/99.92	88.68/202.31/100.40	88.78/201.95/100.11
β (°)	99.186	99.141	99.177
Number of reflections			
Measured	1471142 (145181)	902385 (68612)	2097975 (200889)
Unique	346368 (34567)	212277 (19059)	574432 (57397)
Completeness (%)	99.8 (99.9)	98.2 (88.4)	100.0 (100.0)
R_{merge} (%)	6.2 (37.5)	14.0 (49.0)	7.1 (49.6)
Mean $I/\sigma(I)$	19.1 (2.5)	8.5 (1.6)	20.9 (3.3)
Multiplicity	4.2 (4.2)	4.3 (3.6)	3.7 (3.5)
Refinement			
Number of reflections used	332107 (30562)	197345 (14891)	548128 (49577)
R_{work} (%)	15.1 (21.6)	15.3 (24.0)	15.0 (21.7)
R_{free} (%)	17.6 (23.7)	19.4 (27.6)	16.8 (22.8)
Geometry deviations			
Bond lengths (Å)	0.015	0.015	0.015
Bond angles (°)	1.77	1.78	1.74
Number of atoms/mean B-values (Å^2)			
Protein atoms	20588/16.6	20588/17.3	20588/13.7
Tris atoms	32/13.6	–	–
Xylose atoms	–	–	350/34.1
Xylobiose atoms	–	76/38.3	–
Water molecules	3164/32.9	2518/32.8	3614/34.0
Ramachandran plot (%)			
Most favoured	86.9	86.2	87.4
Additionally allowed	12.7	13.4	12.3
Disallowed	0.4	0.4	0.4

Xylo-oligosaccharides longer than two sugar units will be exposed to the bulk solvent that surrounds the enzyme. The xylobiose-binding site constitutes the -1 and $+1$ subsites, which appear to be necessary and sufficient for XylC catalysis. The kinetic results also indicate that longer substrates (e.g. xylotriose) did not have a lower K_m (results not shown).

The crystal structures show that the XylC protein is folded into two domains (Figure 1C). The major domain is a long parallel β-helix (shown in green) that comprises residues 1–75 and 201–636. This β-helix domain contains six β-helix repeats, and it is surrounded by seven α-helices and five additional β-strands. According to the original definition of a β-helical structure, the first five and the last one repeats are not complete because these repeats at the N- and C-terminus respectively all lack the PB1 strands [27].

The second domain of XylC is a β-sandwich (coloured blue; residues 76–200) composed of two antiparallel β-sheets, a β-hairpin and three short α-helices (Figure 1C). Interestingly, this β-sandwich domain shows an Ig-like fold according to the structural homology search using DALI [28], having the highest Z-score of 3.8 (a Z-score above 2 means significant similarities and these two structures usually correspond to similar folds). These two domains are both involved in the active-site formation and provide interactions for substrate binding.

Some novel features by structural comparison

As mentioned above, XylC is composed of two domains. When XylC is superimposed with other related parallel β-helix proteins (PelC from *Erwinia chrysanthemi* and RGases from *Aspergillus aculeatus*), an extra β-sandwich domain in XylC becomes prominent (Supplementary Figures S2A and S2B at http://www.biochemj.org/bj/448/bj4480401add.htm). Interestingly, this β-sandwich domain is not involved in any protein oligomerization interaction and it is located in a distal side of the enzyme (coloured blue in Supplementary Figure S2C). Nevertheless, this domain is indispensable for the enzyme activity, because it contains the -1 sugar-stacking residue Trp^{113}, located in a loop here (Figure 2A).

As a common feature of the right-handed parallel β-helix domain, the internal amino acids with hydrophobic and polar groups constitute the aliphatic, aromatic and polar stacks within the inner core that maintain the structural stability [29]. Inside the internal of β-helix, an asparagine ladder formed by three or four aspargine residues was often observed in some other structures [27,30,31]. The asparagine ladder is characteristic of parallel β-helix structure, but is not consistently seen in all proteins with this fold. Interestingly, here, the XylC structure contains a much longer asparagine ladder (of nine asparagine residues: Asn^{254}, Asn^{314}, Asn^{338}, Asn^{370}, Asn^{393}, Asn^{416}, Asn^{436}, Asn^{478} and Asn^{530}) than all others that have been reported (Figure 2B).

To understand further whether all GH120 xylosidase enzymes have a longer asparagine ladder or not, sequence alignments of some GH120 enzymes have been carried out. There are 33 proteins that have now been classified to GH120 from the CAZy website. None of these proteins has been characterized, except for *T. saccharolyticum* XylC (TsXylC)

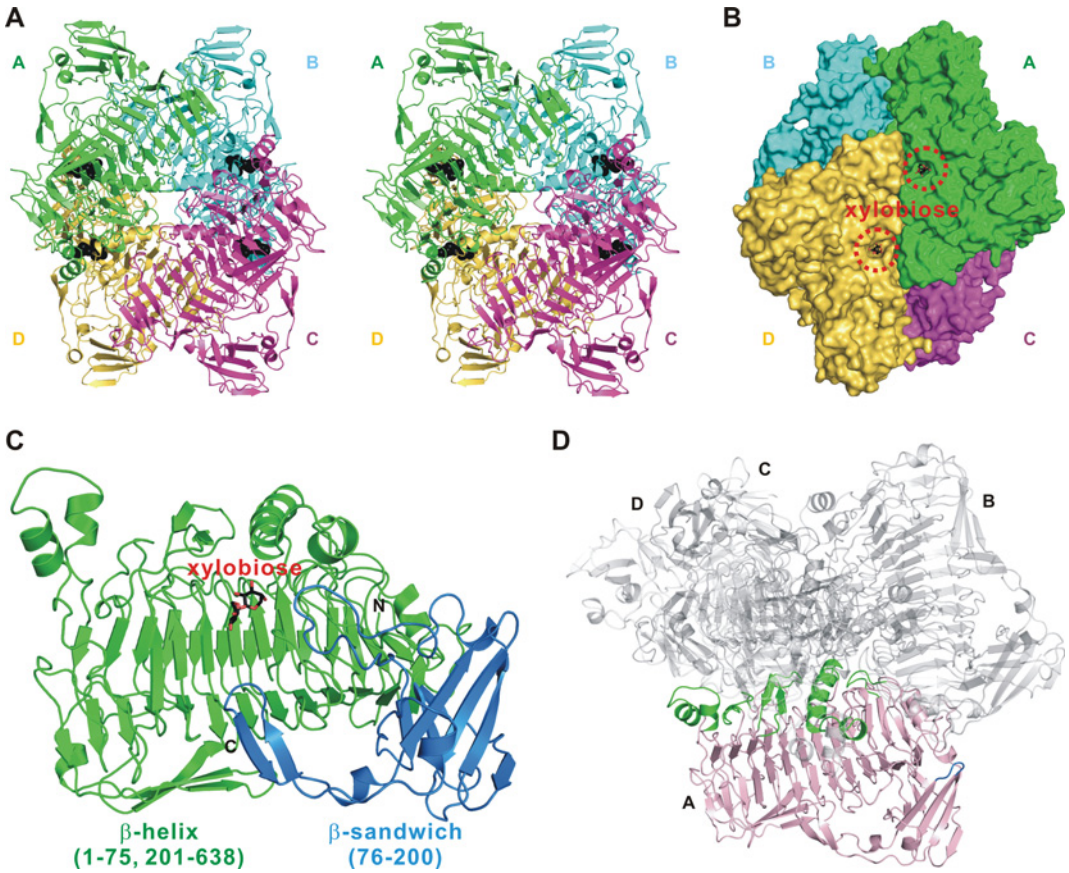

Figure 1 The overall structure of XylC – xylobiose

(**A**) Stereo view of the tetrameric XylC–xylobiose structure. The four monomers are depicted in green, cyan, magenta and yellow; the xylobiose molecules are shown in black sphere representation. (**B**) Surface representation of XylC. (**C**) Two different domains (parallel β-helix in green and β-sandwich domain in blue) of a XylC monomer. (**D**) The regions from the parallel β-helix domain in green (residues 53–59, 276–305, 449–466, 509–519 and 584–596) and one small loop from the β-sandwich domain in blue (residues 177–179) are involved in the tetramer interactions.

and *Bifidobacterium adolescentis* XylB (BaXylB) proteins. The sequences of TsXylC, BaXylB, *Bifidobacterium longum* xylosidase (BlXyl), *Butyrivibrio fibrisolvens* hypothetical protein (BfHyp1), *Acaryochloris marina* hypothetical protein (AmHyp2) and *Roseburia intestinalis* hypothetical protein (RiHyp3), which all belong to the GH120 family, were aligned. TsXylC shares 48 %, 48 %, 40 %, 30 % and 26 % protein identity with BaXylB, BlXyl, BfHyp1, AmHyp2 and RiHyp3 respectively (Supplementary Figure S3 at http://www.biochemj.org/bj/448/bj4480401add.htm). Interestingly, there are indeed longer asparagine ladders (from three to nine asparagine residues) observed among these protein sequences.

XylC shows a higher optimal temperature (65 °C) than for other β-xylosidases in the GH3, GH39 and GH43 families (25–45 °C) [32]. Recently, a new GH120 β-xylosidase B (XylB) having 48 % sequence identity with XylC was purified from *B. adolescentis*, and it was found to have an optimal temperature of 60 °C [33]. The higher thermostability of XylC and BaXylB (with eight asparagine ladder residues) might be attributed not only to the larger β-helix domain, but also to the extensive tetramer interface. The longer asparagine ladder may provide intrinsic interactions to stabilize the β-helix fold and increase the thermostability. Because only two GH120 β-xylosidase enzymes have been characterized to date, more studies are warranted to understand the structure–function relationship in the future.

Active-site interactions

The electron-density maps of the Tris ion and the bound xylobiose and xylose, are all very clear in the -1 subsite (Figures 3A and 3B and Supplementary Figure S4A at http://www.biochemj.org/bj/448/bj4480401add.htm). The Tris ion superimposes very well with the xylose unit bound to the -1 subsite and is stabilized by nine and two hydrogen bonds between the Tris ion and seven protein residues, and the Tris ion and two water molecules respectively (Supplementary Figures S4B and S4C). However, the xylose unit of xylobiose in the $+1$ site is not as clearly seen as in the -1 site because of fewer interactions with the enzyme (Figures 3B and 3C).

From the XylC–xylobiose structure, there are 14 hydrogen bonds formed between the -1 xylose unit and eight amino acid residues, Trp^{113}, Gln^{289}, Glu^{353}, Lys^{358}, His^{360}, Asp^{382}, Trp^{383} and Arg^{450}. In contrast, only two hydrogen bonds between the $+1$ xylose unit and Glu^{405} are observed (Figure 3C). Besides, Trp^{113} and His^{352} provide stacking interactions with the -1 and $+1$ xylopyranose rings respectively.

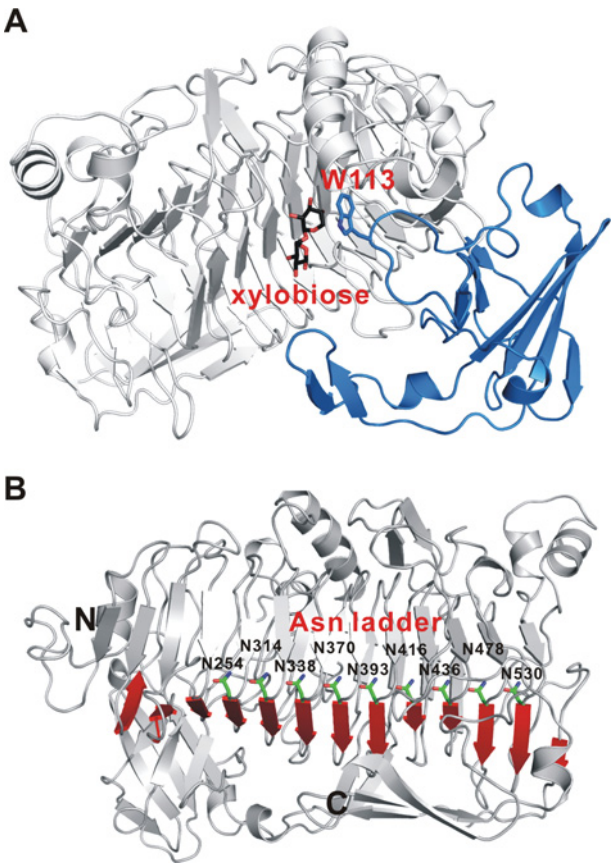

Figure 2 Structure features

(**A**) The β-sandwich domain (in blue) is indispensable for XylC, because Trp^{113} in the loop is important for substrate binding by providing stacking interaction with the xylose unit at the subsite -1. (**B**) XylC has the longest asparagine ladder (nine asparagine residues) of all asparagine ladders observed from parallel β-helix structures solved to date.

To elucidate further the importance of active-site residues, a few amino acids involved in binding xylobiose were mutated and the specific activities were measured (Table 2). The measurement was performed with *p*NP-xylose as an artificial substrate that structurally mimics xylobiose, whereas the hydrolysed product of *p*-nitrophenol (and xylose) is easier to monitor. The results show that the residues involved in the hydrogen bonds with xylobiose are important for catalysis. The mutants E353A, K358A, W380A, D382A, W383A and E405A lost activity completely, but H360A and R450A retained 23.3 % and 37.3 % activity respectively (Table 2). The stacking interactions with the xylopyranose rings are also investigated. The mutant W113A lost all of its enzymatic activity, but the activity was restored when the tryptophan residue was replaced with an alternative aromatic residue (43.8 % activity for W113Y and 97.6 % for W113F). This result indicates that the stacking interaction between Trp^{113} and the -1 xylopyranose ring is essential for substrate binding. Regarding the stacking interaction of H352 with the $+1$ xylopyranose ring, the mutant H352A retained 30.5 % activity (Table 2). We tried to obtain XylC complex structures with longer substrates (e.g. xylotriose) by co-crystallization and soaking methods, but it turned out that only xylobiose density was observed in the active site (results not shown). It is possible that the xylotriose had been hydrolysed to xylobiose. Another, perhaps more likely, possibility is that the third xylose unit was too flexible to be observed, because of the lack of specific interaction for this sugar.

Table 2 Activities of wild-type and mutant XylC

ND, not detectable.

Name	Activity (units/mg)	Relative activity (%)
Wild-type	24.9	100
W113A	ND	–
W113Y	10.9	43.8
W113F	24.3	97.6
H352A	7.6	30.5
E353A	ND	–
K358A	ND	–
H360A	5.8	23.3
W380A	ND	–
D382A	ND	–
W383A	ND	–
E405A	ND	–
R450A	9.3	37.3

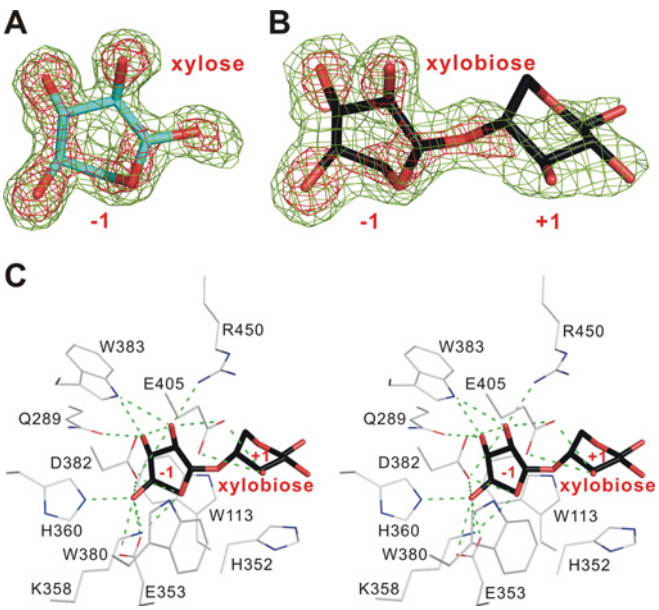

Figure 3 Electron-density maps and the active site

The $2F_o - F_c$ electron-density maps of xylose (**A**) and xylobiose (**B**) are contoured at 1.0σ and 2.5σ levels (in green and red respectively). (**C**) Stereo view of the detailed interaction networks of XylC active-site residues with xylobiose. There are 14 hydrogen bonds (green broken lines) between the active-site residues with the xylose unit at the -1 subsite, but only two hydrogen bonds with the xylose unit at the $+1$ subsite.

Possible mechanisms for catalysis and low product inhibition

All β-xylosidases characterized hydrolyse xylo-oligosaccharides by using two carboxylate residues, such as aspartate and glutamate (GH3 and GH43), glutamate and glutamate (GH30 and GH39), and glutamate and aspartate (GH52 and GH116) as nucleophile and general acid respectively. They are classified according to the two-step retaining and the single-step inverting mechanisms (http://www.cazy.org/Glycoside-Hydrolases.html). At present, only seven β-xylosidase crystal structures of two GH families (GH39 and GH42) were determined and the PDB codes of the structures are 1W91, 2BFG, 2BS9, 1PX8 and 1UHV (GH39), and 1YRZ and 1YIF (GH43). It is not feasible to propose the catalytic mechanism comparing the XylC structure with the available β-xylosidase structures because the active sites are significantly different between GH39 [$(\beta/\alpha)_8$], GH43 (5-fold β-propeller) and GH120 (right-handed parallel β-helix). In XylC, the side chains

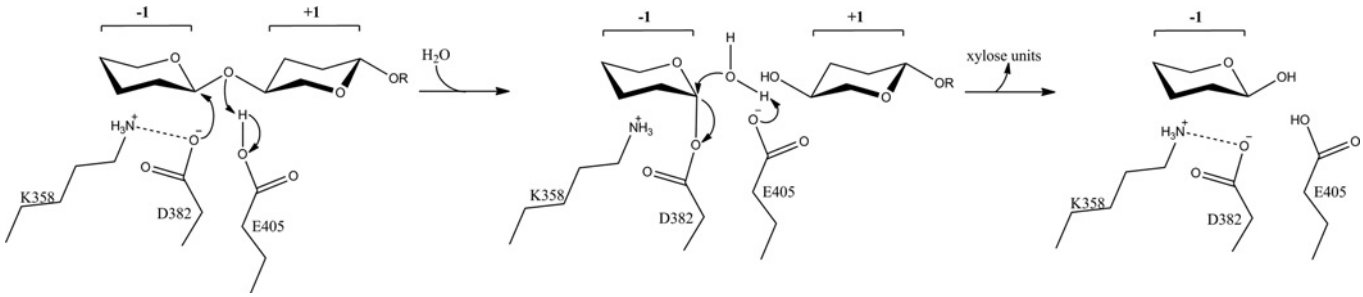

Scheme 1 The proposed catalytic mechanism of XylC

R = xylose.

of Glu^{353}, Asp^{382} and Glu^{405} are all located within an appropriate distance from the xylobiose. However, further analysis shows that Glu^{353} is too far from the anomeric carbon of the -1 xylose (C1B) and the bridging oxygen to the $+1$ xylose (O4A). Thus Glu^{353} is probably not a catalytic residue, but only involved in substrate binding. On the other hand, Asp^{382} is more likely to serve as the nucleophile because it is properly oriented toward the -1 xylose, with the oxygen atoms at 3.1 Å and 2.8 Å from the C1 (C1B) and O2 (O2B) atoms. In addition, hydrogen bonding to the adjacent Lys^{358} side chain ensures that the carboxy oxygen near the C1 atom is negatively charged and ready for nucleophilic attack. After the nucleophilic attack, an acylxylose intermediate is formed, which in turn is hydrolysed by an incoming water molecule, supposed to take over the original place of the O4 (O4A) atom of the $+1$ sugar. In this step, Glu^{405} probably serves as a general acid to subtract a proton from the water. Moreover, the short distance between the Asp^{382} and Glu^{405} of 4.9 Å also suggests that XylC cleaves the glycosidic bond via the retaining pathway rather than the inverting mechanism (Scheme 1). This retaining mechanism is also supported by the results of stereochemical analysis, which showed that XylC produced β-xylose from β-xylopyranosides [4]. From the sequence alignment results, the active-site residues are highly conserved among all these sequences, especially for the two proposed catalytic residues (Asp^{382} and Glu^{405}) (Supplementary Figure S3).

β-Xylosidase is an important enzyme in the final steps of xylan hydrolysis to xylose. Most of the xylosidases known to date exhibit a strong product inhibition by xylose, although it is not so strong for a few recently discovered β-xylosidases from fungi and bacteria, which might possibly be beneficial for industrial use. Examples are the fungal β-xylosidases from *Scytalidium thermophilum* (0 % inhibition at 200 mM xylose), *Humicola grisea* var. *thermoidea* (0 % inhibition at 10 mM) and *Aspergillus nidulans* (44 % inhibition at 25 mM) [4]. On the other hand, bacterial β-xylosidases usually exhibit lower K_i values ranging from 2 to 10 mM xylose [34]. Interestingly, with 70 % activity retained in the presence of 200 mM xylose, XylC has by far the highest xylose tolerance among all the known bacterial β-xylosidases [4].

The XylC–xylose complex crystal (with 200 mM xylose) shows, in addition to the active-site bound xylose molecules (coloured red), 31 other molecules (six observed at the dimer interface) of bound xylose (coloured green), which correspond to nine binding sites consistently present in each monomer (plus one bound to a different site in monomer D, coloured blue) (Figure 4). Despite the diverse interactions in the different sites (Supplementary Figure S5 at http://www.biochemj.org/bj/448/bj4480401add.htm), these well-defined symmetrically distributed binding sites in the XylC tetramer are probably specific for xylose. These findings suggest a working hypothesis for future investigation, that the presence of 'allosteric' xylose-binding sites on XylC may attract free xylose to reduce the local product concentration and it can be related to the observed high tolerance against product inhibition. This hypothesis, however, still needs to be verified by further studies.

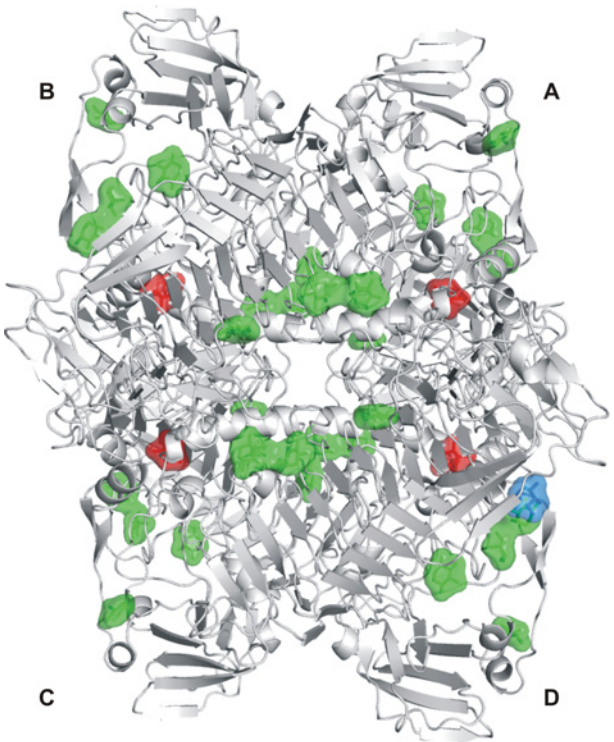

Figure 4 Xylose-binding sites from the XylC–xylose structure

Four xyloses in the active site are shown in red and 31 reproducible xyloses bound to the other additional sites are shown in green. The non-specific site is shown in blue.

ACKNOWLEDGEMENTS

The synchrotron data collection was conducted at beamline BL13B1 of NSRRC (National Synchrotron Radiation Research Center, Taiwan) supported by the National Science Council

of Taiwan, and at beamline BL17U of the Shanghai Synchrotron Radiation Facility (SSRF, Shanghai, China).

FUNDING

This work was supported by the National High Technology Research and Development Program of China [grant number 2012AA022200 (to R.-T.G.)], the National Basic Research Program of China [grant number 2011CB710800 (to R.-T.G.)] and the National Natural Science Foundation of China [grant number 30970062 (to W.S.)].

REFERENCES

1 Saha, B. C. (2003) Hemicellulose bioconversion. J. Ind. Microbiol. Biotechnol. **30**, 279–291
2 Biely, P. (1985) Microbial xylanolytic systems. Trends Biotechnol. **3**, 286–290
3 Cantarel, B. L., Coutinho, P. M., Rancurel, C., Bernard, T., Lombard, V. and Henrissat, B. (2009) The Carbohydrate-Active EnZymes database (CAZy): an expert resource for glycogenomics. Nucleic Acids Res. **37**, D233–D238
4 Shao, W., Xue, Y., Wu, A., Kataeva, I., Pei, J., Wu, H. and Wiegel, J. (2011) Characterization of a novel β-xylosidase, XylC, from *Thermoanaerobacterium saccharolyticum* JW/SL-YS485. Appl. Environ. Microbiol. **77**, 719–726
5 Shao, W., Deblois, S. and Wiegel, J. (1995) A high-molecular-weight, cell-associated xylanase isolated from exponentially growing *Thermoanaerobacterium* sp. strain JW/SL-YS485. Appl. Environ. Microbiol. **61**, 937–940
6 Shao, W., Obi, S., Puls, J. and Wiegel, J. (1995) Purification and characterization of the α-glucuronidase from *Thermoanaerobacterium* sp. strain JW/SL-YS485, an important enzyme for the utilization of substituted xylans. Appl. Environ. Microbiol. **61**, 1077–1081
7 Shao, W. and Wiegel, J. (1995) Purification and characterization of two thermostable acetyl xylan esterases from *Thermoanaerobacterium* sp. strain JW/SL-YS485. Appl. Environ. Microbiol. **61**, 729–733
8 Lorenz, W. W. and Wiegel, J. (1997) Isolation, analysis, and expression of two genes from *Thermoanaerobacterium* sp. strain JW/SL YS485: a β-xylosidase and a novel acetyl xylan esterase with cephalosporin C deacetylase activity. J. Bacteriol. **179**, 5436–5441
9 Liu, W., Sun, Y., Ko, T. P., Wiegel, J., Shao, W., Lu, F., Guo, R. T. and Huang, C. H. (2012) Crystallization and preliminary X-ray diffraction analysis of a novel GH120 β-xylosidase (XylC) from *Thermoanaerobacterium saccharolyticum* JW/SL-YS485. Acta Crystallogr. Sect. F Struct. Biol. Cryst. Commun. **68**, 914–916
10 Otwinowski, Z. and Minor, W. (1997) Processing of X-ray diffraction data collected in oscillation mode. Methods Enzymol. **276**, 307–326
11 Brunger, A. T. (1993) Assessment of phase accuracy by cross validation: the free R value: methods and applications. Acta Crystallogr. Sect. D Biol. Crystallogr. **49**, 24–36
12 Guo, R. T., Kuo, C. J., Chou, C. C., Ko, T. P., Shr, H. L., Liang, P. H. and Wang, A. H. (2004) Crystal structure of octaprenyl pyrophosphate synthase from hyperthermophilic *Thermotoga maritima* and mechanism of product chain length determination. J. Biol. Chem. **279**, 4903–4912
13 Sun, H. Y., Ko, T. P., Kuo, C. J., Guo, R. T., Chou, C. C., Liang, P. H. and Wang, A. H. (2005) Homodimeric hexaprenyl pyrophosphate synthase from the thermoacidophilic crenarchaeon *Sulfolobus solfataricus* displays asymmetric subunit structures. J. Bacteriol. **187**, 8137–8148
14 Cheng, Y. S., Ko, T. P., Wu, T. H., Ma, Y., Huang, C. H., Lai, H. L., Wang, A. H., Liu, J. R. and Guo, R. T. (2011) Crystal structure and substrate-binding mode of cellulase 12A from *Thermotoga maritima*. Proteins **79**, 1193–1204
15 Ren, F., Ko, T. P., Feng, X., Huang, C. H., Chan, H. C., Hu, Y., Wang, K., Ma, Y., Liang, P. H., Wang, A. H. et al. (2012) Insights into the mechanism of the antibiotic-synthesizing enzyme MoeO5 from crystal structures of different complexes. Angew. Chem. Int. Ed. **51**, 4157–4160
16 Terwilliger, T. C. and Berendzen, J. (1999) Automated MAD and MIR structure solution. Acta Crystallogr. Sect. D Biol. Crystallogr. **55**, 849–861
17 Terwilliger, T. C. (2000) Maximum-likelihood density modification. Acta Crystallogr. Sect. D Biol. Crystallogr. **56**, 965–972
18 Terwilliger, T. C. (2003) Automated main-chain model building by template matching and iterative fragment extension. Acta Crystallogr. Sect. D Biol. Crystallogr. **59**, 38–44
19 Terwilliger, T. C. (2003) SOLVE and RESOLVE: automated structure solution and density modification. Methods Enzymol. **374**, 22–37
20 Murshudov, G. N., Vagin, A. A. and Dodson, E. J. (1997) Refinement of macromolecular structures by the maximum-likelihood method. Acta Crystallogr. Sect. D Biol. Crystallogr. **53**, 240–255
21 Perrakis, A., Morris, R. and Lamzin, V. S. (1999) Automated protein model building combined with iterative structure refinement. Nat. Struct. Biol. **6**, 458–463
22 McCoy, A. J., Grosse-Kunstleve, R. W., Adams, P. D., Winn, M. D., Storoni, L. C. and Read, R. J. (2007) Phaser crystallographic software. J. Appl. Crystallogr. **40**, 658–674
23 Emsley, P. and Cowtan, K. (2004) Coot: model-building tools for molecular graphics. Acta Crystallogr. Sect. D Biol. Crystallogr. **60**, 2126–2132
24 Brunger, A. T., Adams, P. D., Clore, G. M., DeLano, W. L., Gros, P., Grosse-Kunstleve, R. W., Jiang, J. S., Kuszewski, J., Nilges, M., Pannu, N. S. et al. (1998) Crystallography & NMR system: a new software suite for macromolecular structure determination. Acta Crystallogr. Sect. D Biol. Crystallogr. **54**, 905–921
25 Krissinel, E. and Henrick, K. (2007) Inference of macromolecular assemblies from crystalline state. J. Mol. Biol. **372**, 774–797
26 Huang, J. W., Cheng, Y. S., Ko, T. P., Lin, C. Y., Lai, H. L., Chen, C. C., Ma, Y., Zheng, Y., Huang, C. H., Zou, P. et al. (2012) Rational design to improve thermostability and specific activity of the truncated *Fibrobacter succinogenes* 1,3-1,4-β-D-glucanase. Appl. Microbiol. Biotechnol. **94**, 111–121
27 Yoder, M. D., Lietzke, S. E. and Jurnak, F. (1993) Unusual structural features in the parallel β-helix in pectate lyases. Structure **1**, 241–251
28 Dietmann, S., Park, J., Notredame, C., Heger, A., Lappe, M. and Holm, L. (2001) A fully automatic evolutionary classification of protein folds: Dali Domain Dictionary version 3. Nucleic Acids Res. **29**, 55–57
29 Jenkins, J. and Pickersgill, R. (2001) The architecture of parallel β-helices and related folds. Prog. Biophys. Mol. Biol. **77**, 111–175
30 Kobe, B. and Deisenhofer, J. (1995) Proteins with leucine-rich repeats. Curr. Opin. Struct. Biol. **5**, 409–416
31 Zheng, Y., Huang, C. H., Liu, W., Ko, T. P., Xue, Y., Zhou, C., Guo, R. T. and Ma, Y. (2012) Crystal structure and substrate-binding mode of a novel pectate lyase from alkaliphilic *Bacillus* sp. N16-5. Biochem. Biophys. Res. Commun. **420**, 269–274
32 Jordan, D. B. and Wagschal, K. (2010) Properties and applications of microbial β-D-xylosidases featuring the catalytically efficient enzyme from *Selenomonas ruminantium*. Appl. Microbiol. Biotechnol. **86**, 1647–1658
33 Lagaert, S., Pollet, A., Delcour, J. A., Lavigne, R., Courtin, C. M. and Volckaert, G. (2011) Characterization of two β-xylosidases from *Bifidobacterium adolescentis* and their contribution to the hydrolysis of prebiotic xylooligosaccharides. Appl. Microbiol. Biotechnol. **92**, 1179–1185
34 Yan, Q. J., Wang, L., Jiang, Z. Q., Yang, S. Q., Zhu, H. F. and Li, L. T. (2008) A xylose-tolerant β-xylosidase from *Paecilomyces thermophila*: characterization and its co-action with the endogenous xylanase. Bioresour. Technol. **99**, 5402–5410

Received 30 August 2012/20 September 2012; accepted 20 September 2012
Published as BJ Immediate Publication 20 September 2012, doi:10.1042/BJ20121359

Biochem. J. (2012) **448**, 401–407 (Printed in Great Britain) doi:10.1042/BJ20121359

SUPPLEMENTARY ONLINE DATA

The substrate/product-binding modes of a novel GH120 β-xylosidase (XylC) from *Thermoanaerobacterium saccharolyticum* JW/SL-YS485

Chun-Hsiang HUANG*[1], Yu SUN†[1], Tzu-Ping KO‡, Chun-Chi CHEN§, Yingying ZHENG*, Hsiu-Chien CHAN*, Xuefei PANG*, Juergen WIEGEL‖[2], Weilan SHAO†[2] and Rey-Ting GUO*[2]

*Industrial Enzymes National Engineering Laboratory, Tianjin Institute of Industrial Biotechnology, Chinese Academy of Sciences, Tianjin 300308, China, †Biofuels Institute, School of Environment, Jiangsu University, Zhenjiang 212013, China, ‡Institute of Biological Chemistry, Academia Sinica, Taipei 11529, Taiwan, §CAS Key Laboratory of Pathogenic Microbiology and Immunology, Institute of Microbiology, Chinese Academy of Sciences, Beijing 100101, China, and ‖Department of Microbiology, University of Georgia, Athens, GA 30602-2605, U.S.A.

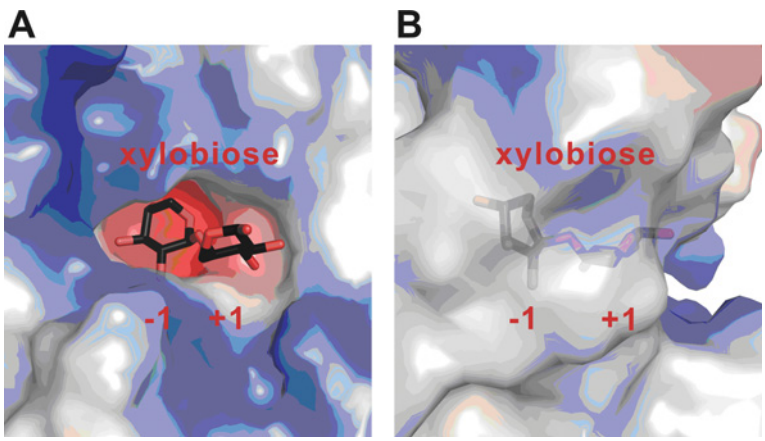

Figure S1 Surface representation of the xylobiose-binding site

(**A**) Electrostatic potential (blue, positive; red, negative) representation of XylC. The xylobiose is shown as sticks and coloured black. (**B**) A 90° rotation view along the vertical axis, showing clearly that the catalytic cavity is suitable for two xylose units.

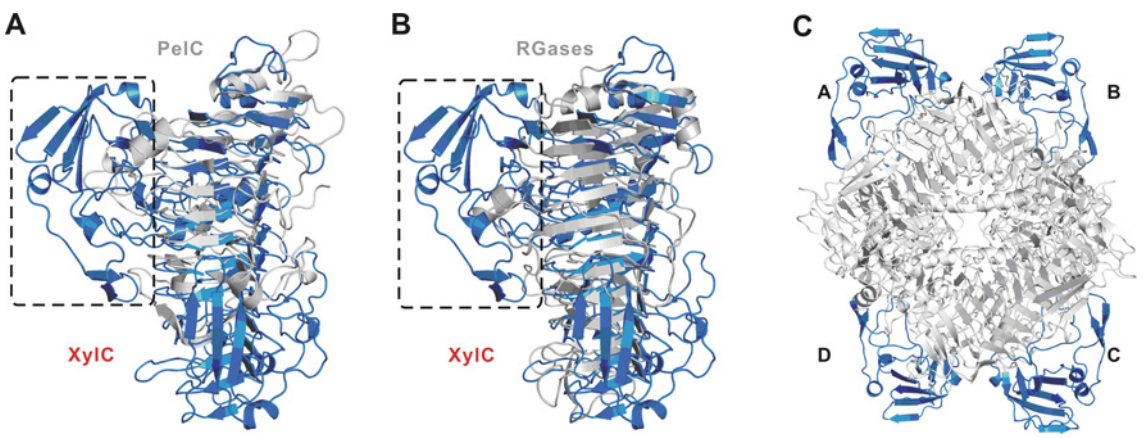

Figure S2 Comparison of XylC with other parallel β-helix folded proteins

(**A** and **B**) The comparison of XylC with PelC (coloured grey, PDB code 1AIR) and RGases (coloured grey, PDB code 1RMG), shows clearly that XylC has an extra β-sandwich domain (broken box). (**C**) This extra domain did not provide any oligomer interactions and is located at the outer region (coloured blue).

[1] These authors contributed equally to this work.

[2] Correspondence may be addressed to any of these authors (email juergenwiegel@gmail.com, weilanshao@gmail.com or guo_rt@tib.cas.cn).

The atomic co-ordinates and structural factors for the wild-type *Thermoanaerobacterium saccharolyticum* JW/SL-YS485 XylC in complex with Tris (code 3VST), xylobiose (code 3VSU) and xylose (code 3VSV) have been deposited in the RCSB PDB.

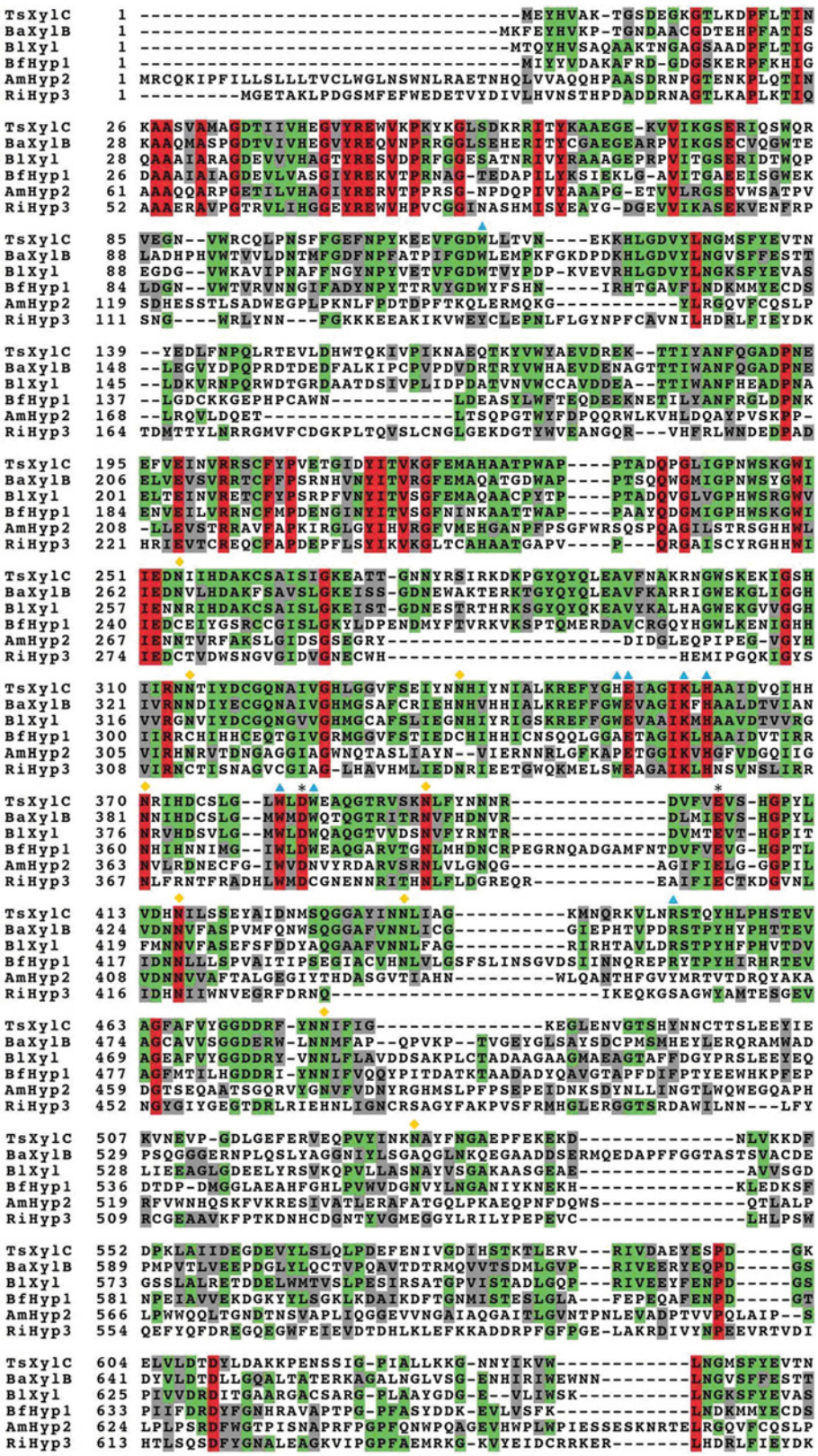

Figure S3 Multiple sequence alignment

Some GH120 family protein sequences, including XylC, XylB, Xyl, Hyp1, Hyp2 and Hyp3 from *T. saccharolyticum* JW/SL-YS485, *B. adolescentis* (ATCC-15703), *B. longum* (KACC-91563), *B. fibrisolvens*, *A. marina* (MBIC-11017) and *R. intestinalis* were aligned. The abbreviation Hyp refers to hypothetical protein with unknown function. Completely conserved residues are shown in red, partially identical residues are shown in green, similar residues are shown in grey. Two catalytic residues (Asp^{382} and Glu^{405}), the substrate-binding residues (Trp^{113}, His^{352}, Glu^{353}, Lys^{358}, His^{360}, Trp^{380}, Trp^{383} and Arg^{450}) and asparagine ladder residues (Asn^{254}, Asn^{314}, Asn^{338}, Asn^{370}, Asn^{393}, Asn^{416}, Asn^{436}, Asn^{478} and Asn^{530}) are indicated by black stars, cyan triangles and orange diamonds respectively.

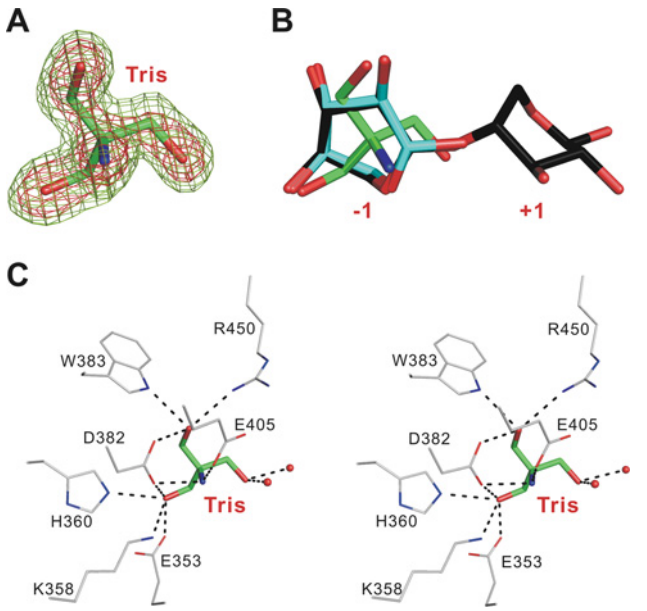

Figure S4 Tris-binding site

(**A**) The $2F_o - F_c$ electron-density map of the Tris ion (contoured at 1.0σ and 2.5σ levels; green and red respectively). (**B**) The Tris ion was superimposed with the xylose and the xylobiose from the complex structures solved in the present study. (**C**) The detailed interaction network of Tris and active-site residues is shown in stereo view. The Tris ion occupies the -1 subsite. There are nine hydrogen bonds between the Tris ion and active-site residues. Two water molecules interact with the Tris ions (shown as red spheres).

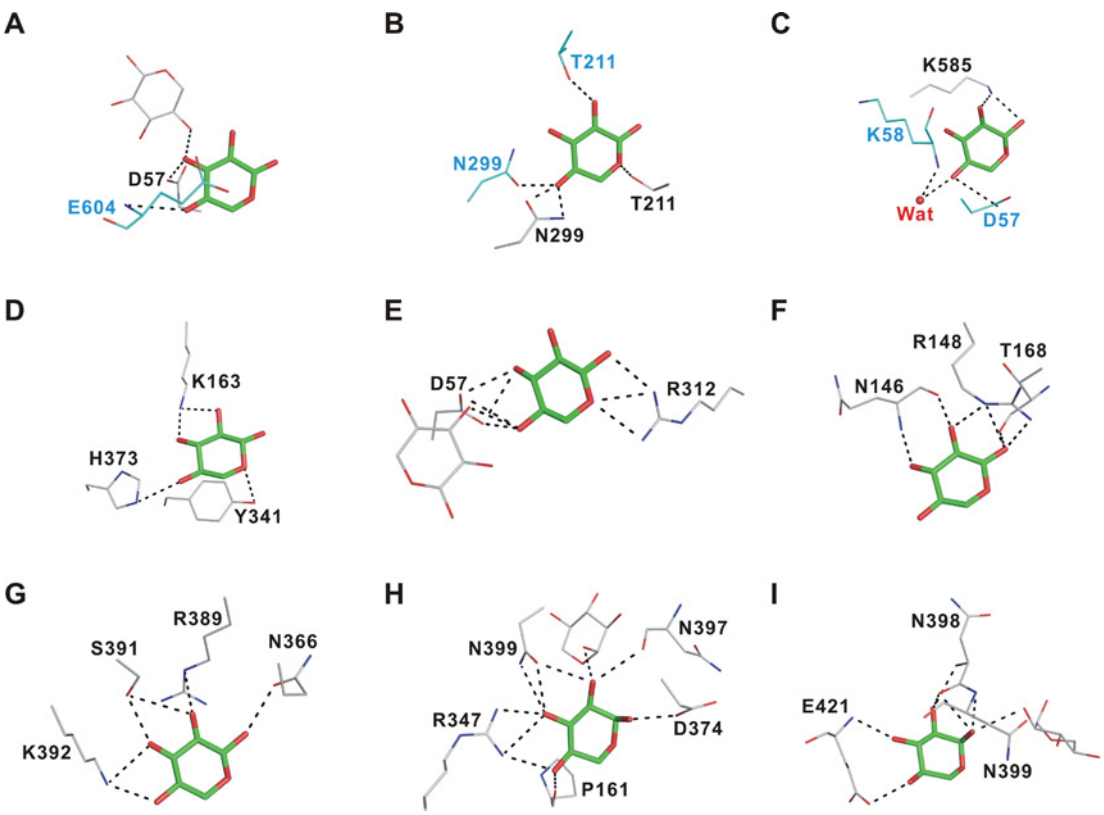

Figure S5 The other xylose-binding sites

(**A**–**I**) From these binding sites, XylC interacted with xylose by side chains and backbone atoms of the residues below, including Asp^{57}, Asn^{146}, Arg^{148}, Pro^{161}, Lys^{163}, Thr^{168}, Thr^{211}, Asn^{299}, Arg^{312}, Tyr^{341}, Arg^{347}, Asn^{366}, His^{373}, Asp^{374}, Arg^{389}, Ser^{391}, Lys^{392}, Asn^{397}, Asn^{398}, Asn^{399}, Glu^{421} and Lys^{585}. The xylose-interacting residues from other monomers are coloured cyan.

Table S1 Summary of mercury-derived protein data collection and phasing statistics

Values in parentheses are for the highest resolution shell. $R_{merge} = \Sigma_{hkl}\Sigma_i|I_i(hkl) - <I(hkl)>|\Sigma_{hkl}\Sigma_i I_i(hkl)$.

Parameter	Wild-type	XylC-$C_{13}H_{17}HgNO_6$	XylC-$Hg(OOCCH3)_2$	XylC-$C_8H_8HgO_2$	XylC-$C(HgOOCCH_3)_4$
Data collection					
Wavelength (Å)	1.0	1.0	1.0	1.0	1.0
Resolution (Å)	25–2.2 (2.28–2.2)	25–2.1 (2.18–2.1)	25–2.1 (2.18–2.1)	25–2.5 (2.59–2.5)	25–2.5 (2.59–2.5)
Space group			$P2_1$		
Unit cell					
a (Å)	88.36	88.54	88.73	88.64	88.68
b (Å)	202.20	201.91	202.99	201.72	202.13
c (Å)	99.87	99.98	100.27	100.12	100.03
β (°)	99.04	99.234	99.14	99.127	99.893
Number of measured reflections	669429 (55187)	1524309 (152007)	832838 (78893)	413232 (412170)	417484 (41359)
Number of unique reflections	173739 (17246)	200423 (20001)	200799 (20229)	117763 (11785)	118316 (11817)
Completeness (%)	99.8 (99.2)	99.9 (100)	98.8 (99.6)	99.4 (99.9)	99.8 (99.9)
R_{merge} (%)	14.6 (41.9)	11.4 (27.3)	13.3 (58.5)	9.8 (38.3)	16.8 (39.0)
Mean $I/\sigma(I)$	11.6 (3.1)	30.8 (9.1)	11.9 (2.4)	14.1 (3.2)	16.7 (4.0)
Multiplicity	3.9 (3.2)	7.6 (7.6)	4.1 (3.9)	3.5 (3.5)	3.5 (3.5)
Phasing					
Number of sites			16		
Z-score			61.53		
Figure of merit			0.72		

Received 30 August 2012/20 September 2012; accepted 20 September 2012
Published as BJ Immediate Publication 20 September 2012, doi:10.1042/BJ20121359